nature geoscience

ARTICLES

PUBLISHED ONLINE: 12 DECEMBER 2016 | DOI: 10.1038/NGEO2863

Centennial glacier retreat as categorical evidence of regional climate change

Gerard H. Roe[1]*, Marcia B. Baker[1] and Florian Herla[2]

The near-global retreat of glaciers over the last century provides some of the most iconic imagery for communicating the reality of anthropogenic climate change to the public. Surprisingly, however, there has not been a quantitative foundation for attributing the retreats to climate change, except in the global aggregate. This gap, between public perception and scientific basis, is due to uncertainties in numerical modelling and the short length of glacier mass-balance records. Here we present a method for assessing individual glacier change based on the signal-to-noise ratio, a robust metric that is insensitive to uncertainties in glacier dynamics. Using only meteorological and glacier observations, and the characteristic decadal response time of glaciers, we demonstrate that observed retreats of individual glaciers represent some of the highest signal-to-noise ratios of climate change yet documented. Therefore, in many places, the centennial-scale retreat of the local glaciers does indeed constitute categorical evidence of climate change.

Alpine glaciers are consequential and captivating elements of the Earth system that feature prominently in the lives of nearby communities[1]. The nature of glacier motion was a research challenge for nineteenth-century physicists[2,3], and the late Holocene history of glacier margins has been a primary target of modern palaeoclimate science[4]. Consequently, the century-scale length history of several hundred glaciers is well known (for example, Fig. 1)[4,5]. Whilst glacier mass balance (that is, area-averaged accumulation minus ablation, $\equiv b$ (m yr^{-1})) is a more direct measure of climate[6,7] than glacier length, only a few dozen mass-balance records extend for more than two decades.

The century-scale, near-global retreat of glacier fronts seems improbable without some coordinating global climate change. However, the formal statistical assessment of the role of climate change in glacier retreat has been limited to the numerical modelling of three individual glaciers, each with only a single set of model parameters[8]; and to a comparison of the global aggregate glacier mass loss in forced and unforced integrations of global climate models[9].

By itself, any single glacier is a blunt statistical instrument. Each is a unique product of its local climate and landscape. Characteristic glacier-length response times of several decades[10] imply only a few independent degrees of freedom in a centennial record, resulting in poor statistical resolving power to evaluate a trend. In part because of these factors, the most recent assessment of the Intergovernmental Panel on Climate Change (IPCC) concluded only it was 'likely' that a 'substantial' part of glacier retreat is due to anthropogenic climate change, a much weaker attribution than for other metrics of climate change[11]. Here we introduce a method to combine glacier observations with the better-resolved local meteorological trends, which facilitates strong conclusions. The centennial-scale retreats of 37 widely dispersed glaciers have each necessarily required a climate change. And while the cause cannot be attributed purely from observations, the required climate changes are centennial-scale trends that are globally distributed.

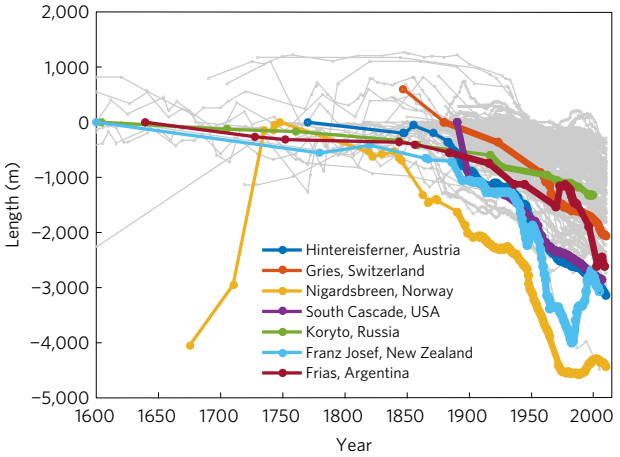

Figure 1 | The global record of glacier lengths[5], for 158 glaciers with 20 or more individual observations (shown as dots). Coloured lines show the specific glaciers analysed in Fig. 4.

The signal-to-noise ratio as a metric of glacier change

We relate s_L, the signal-to-noise ratio of glacier length ($\equiv L$), to s_b, the signal-to-noise ratio of mass balance ($\equiv b$). Let ΔL be the change in length over some period of time, and let σ_L be the standard deviation in the absence of any climate trend. Then $s_L \equiv \Delta L/\sigma_L$. Likewise, $s_b \equiv \Delta b/\sigma_b$. We first establish that s_L is straightforwardly related to s_b, and that the relationship is insensitive to uncertainties in glacier parameters. The result is robust and depends only on the fundamental property that glaciers integrate mass balance on timescales of a few decades.

In a refinement of earlier models[12,13], previous work has shown that glacier flow on a sloping bed can be accurately emulated by a linear, third-order differential equation (Methods)[14]. Let $\Delta b(t_o)$ be the change in mass balance due to a linear trend applied over a

[1]Department of Earth and Space Sciences, University of Washington, Seattle, Washington 98195, USA. [2]Institute of Atmospheric and Cryospheric Sciences, University of Innsbruck, A-6020 Innsbruck, Austria. *e-mail: gerard@ess.washington.edu

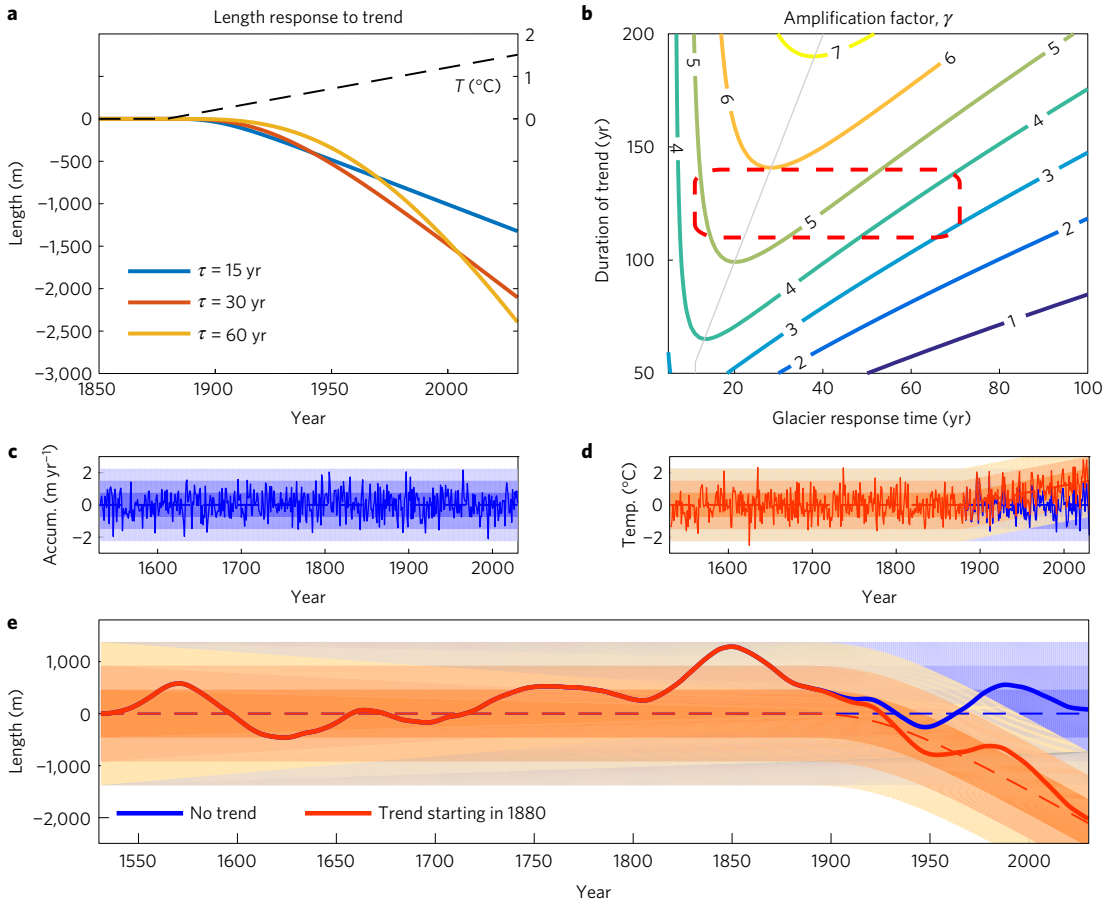

Figure 2 | The response of idealized glaciers to climate. a, The response to a warming trend (dashed line, right axis) of three idealized glaciers with response times of $\tau = 15$, 30 and 60 yr (coloured lines, left axis). **b**, The amplification factor $\gamma(\tau, t_o)$, in the relationship $s_L = \gamma \cdot s_b$. The dashed red box covers the approximate range applicable to alpine glaciers. Thus, $\gamma \simeq 4$ to 6 for a wide range of the relevant parameter space. **c**, A 500-yr segment of synthetic, random white-noise accumulation ($\sigma_P = 0.75$ m yr^{-1}), shading denotes 1, 2 and 3σ ranges. **d**, As for **c**, but for melt-season temperature ($\sigma_T = 0.75$ °C), and with an imposed 1 °C-per-century warming trend beginning in 1880. The blue line and shading have no warming trend. **e**, Response of a glacier with $\tau = 30$ yr, $\beta = 180$. Due to the applied warming trend from 1880 to 2010, $\Delta L = -1{,}700$ m, $\sigma_L = 460$ m, giving $s_L = -3.7$. In these simulations, anomalies in temperature and mass balance are related via $b' = -\mu T'$, with $\mu = 0.65$ m yr^{-1} °C^{-1}.

period t_o. Our model yields $\Delta L(t_o) = \phi(t_o, \tau) \cdot \beta \cdot \Delta b(t_o)$, where τ and β are functions of glacier geometry. The glacier response time $\tau = -H/b_t$, where H is a characteristic ice thickness and b_t is the (negative) mass balance at the terminus[12]; β is the ratio of the glacier area to the product of H and the width across the terminus. The function $\phi(t_o, \tau)$ embodies the ice dynamics, and captures three distinct stages of adjustment: changes in interior ice thickness drive changes in ice flux at the terminus that, in turn, drive changes in glacier length[12,14]. τ is central to a glacier's response: Fig. 2a shows $\Delta L(t)$ for a warming trend of 1 °C per century, for three glaciers with different τ (and fixed β). Physically, τ controls how quickly a glacier responds to climate variations and also how strongly the glacier is restored to equilibrium[12–14]: small-τ glaciers respond quickly but are less sensitive, whereas large-τ glaciers respond slowly but are ultimately more sensitive. These fundamental trade-offs are independent of the model used (see Supplementary Information), and mean that a century or so after a climate trend commences, the amount of retreat is relatively insensitive to several-fold variations in τ (Fig. 2a).

Our model, and all equivalent models, also yield $\sigma_L \propto \beta \cdot \sigma_b$ (Methods). Thus, s_L can be written as:

$$s_L = \gamma(t_o, \tau) \cdot s_b \quad (1)$$

$\gamma(t_o, \tau)$ is an amplification factor that depends only on the duration of the trend and the glacier response time. The counteracting tendencies of initial responsiveness versus long-term sensitivity mean that $\gamma(t_o, \tau)$ is quite insensitive to τ. For example, for a 130-yr trend, glacier length is a fourfold to sixfold amplifier of the mass-balance signal-to-noise ratio, across a wide range of response times (Fig. 2b). The relative constancy of γ is key to estimating s_L from meteorological observations. Note both ΔL and σ_L are proportional to the parameter β and so it drops out of s_L.

The relationship between s_L and s_b can be illustrated with a synthetic example for typical climate trends and variability. Assume a 1 °C-per-century increase in melt-season (June–September) temperature ($\equiv T$) beginning in 1880, no trend in annual-mean precipitation ($\equiv P$), and white-noise interannual variability (consistent with observations[7]) characterized by $\sigma_T = 0.75$ °C and $\sigma_P = 0.75$ m yr^{-1}, respectively (Fig. 2c,d). A simple mass-balance model is $b' = P' - \mu T'$, where μ is a melt factor ($= 0.65$ m yr^{-1} K^{-1})[15], and primes denote fluctuations about the long-term mean. After 130 yr of the imposed trend, $s_b = -0.65$. For $\tau = 30$ yr and $\beta = 180$, we get $\Delta L = -1{,}700$ m and $\sigma_L = 460$ m (Fig. 2e). Thus, the retreat is approximately three-and-a-half standard deviations ($s_L = \Delta L/\sigma_L \simeq -3.5$), consistent with an amplification factor of $\gamma \simeq 5.7$ (equation (1) and Fig. 2b).

An application to Hintereisferner, Austria

We next present the steps of our analysis for Hintereisferner in the Austrian Alps (Fig. 1). Applying least-squares regression for the

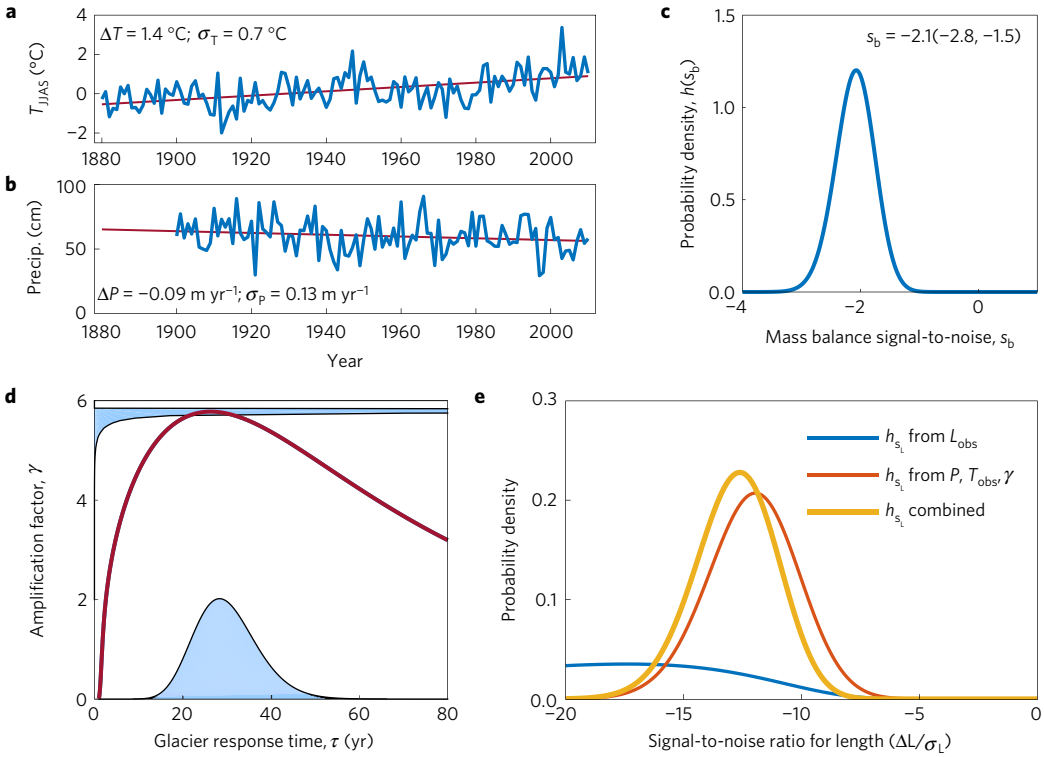

Figure 3 | Analysis for Hintereisferner (Austrian Alps, 46.8° N, 10.8° E). a, Melt-season (June–September) temperature from the Berkeley Earth data set of gridded station observations[17]. The best-fit trend, the change since 1880 and the standard deviation are also shown. **b**, As for **a**, but from the Legates and Willmot data set of gridded annual-mean precipitation[18], with the trend extrapolated to 1880. **c**, The PDF of the signal-to-noise ratio for mass balance, s_b (equation (2)), with median and 95% bounds also given. **d**, The blue shading on the *x* axis shows the PDF of uncertainty in glacier response time, τ; the red curve shows the relationship between τ and the amplification factor, γ, for a 130-yr trend; the blue shading on the *y* axis shows the PDF for γ that results from the PDF for τ being projected onto the y axis via the red line. **e**, PDFs of length signal-to-noise ratio, s_L, from different methods: blue, s_L from observations of *L*; red, s_L from *T*, *P* observations and the amplification factor γ (that is, equation (1)); orange, combined PDF using Bayes' theorem.

period 1880–2010, the glacier retreated 2,800 m with a standard deviation of 130 m about that trend. However, there are only three effective degrees of freedom in the record (Methods), so neither ΔL nor σ_L is well constrained. Consequently, the probability density function (PDF) of their ratio ($\equiv h_{s_L}|^{L_{obs}}$) is very broad (Fig. 3e and Methods): while it is extremely unlikely (<1%) that $s_L > 0$, one cannot rule out the possibility its magnitude is very large (that is, $s_L < -20$). In other words, there is not much information about s_L from the glacier length alone.

An independent approach to calculating s_L uses equation (1). To that end, we build a simple mass-balance model using long-duration, gridded instrumental observations[16,17] of *T* and *P*, scaled by the observed variability of the much shorter winter (b_w) and summer (b_s) mass-balance records[7,18]:

$$b'(t) = b'_w(t) + b'_s(t) = \sigma_{b_w}\frac{P'(t)}{\sigma_P} + \sigma_{b_s}\frac{T'(t)}{\sigma_T} \quad (2)$$

where $\sigma_{(x)}$ is the standard deviation of x. Thus, the modelled mass balance matches the observed variance, and combines the observed signal-to-noise ratios of *P* and *T*. Normalizing by σ_P accounts for orographic-precipitation effects since fractional variations in precipitation are relatively uniform in mountainous areas. Between 1880 and 2010, Hintereisferner experienced strong warming: $\Delta T = +1.4\,^{\circ}\mathrm{C}$, with $\sigma_T = 0.7\,^{\circ}\mathrm{C}$ (Fig. 3a); and some drying: $\Delta P = -0.09\,\mathrm{m\,yr^{-1}}$, with $\sigma_P = 0.13\,\mathrm{m\,yr^{-1}}$ (Fig. 3b, extrapolated from a 100-yr record). Observations from the adjacent Vernagtferner[18] give $\sigma_{b_w} = 0.22\,\mathrm{m\,yr^{-1}}$, $\sigma_{b_s} = 0.42\,\mathrm{m\,yr^{-1}}$. Thus, from equation (2), the median (and 95% bounds) for $s_b = -2.1(-2.8, -1.5)$ (Fig. 3c and Methods): s_b is negative but with some uncertainty. Although the detrended $b'(t)$ is consistent with white noise, we evaluate the potential impact of climatic persistence in the Supplementary Information.

For Hintereisferner[19], $H \simeq 170\,\mathrm{m}$ and $b_t \simeq -6\,\mathrm{m\,yr^{-1}}$, giving $\tau \simeq 30\,\mathrm{yr}$. Formulae for τ vary in the literature[12,13], so we allow broad uncertainty; we represent its PDF by a gamma distribution with $\sigma_\tau = \tau/4$. Figure 3d shows this nonetheless results in a very narrow PDF of γ, centred on $\gamma \simeq 5.6$. Hintereisferner thus acts as a near-optimal amplifier of the climate signal-to-noise ratio. From equation (1) the PDFs of γ and s_b can be combined to give a second PDF for s_L ($\equiv h_{s_L}|^{T,P_{obs}}$), based only on instrumental observations and the approximately several-decade response time of this glacier (Fig. 3e). This PDF rules out extremely negative s_L (for example, $s_L \leq -20$) as inconsistent with observed climate trends (that is, $s_b \simeq -2$) and the roughly sixfold amplification by the glacier length.

These two PDFs of s_L, one based on observations of *L*, and one based on γ and s_b, are independent. Therefore, they can be combined using Bayes' theorem (Methods)[20]. The resulting median (and 95% bounds) is $s_L = -13(-17, -10)$ (Fig. 3e). This is an extraordinarily large magnitude compared with other documented climate metrics. For comparison, the local ΔT near Hintereisferner is 2σ, and the global-mean, annual-mean ΔT trend over the same period is 6σ.

The result that $\Delta L \approx -13\sigma_L$ must not itself be directly equated to statistical significance because length variations are correlated in time. To proceed, we solve for the PDF of σ_L from the relation $\sigma_L = \Delta L|^{obs}/s_L$, using the known observed retreat and the combined PDF for s_L. For Hintereisferner, we find σ_L (and 95% bounds) = 220(170, 280) m. Although this estimate depends primarily on observations, it is consistent with calculations from modelling

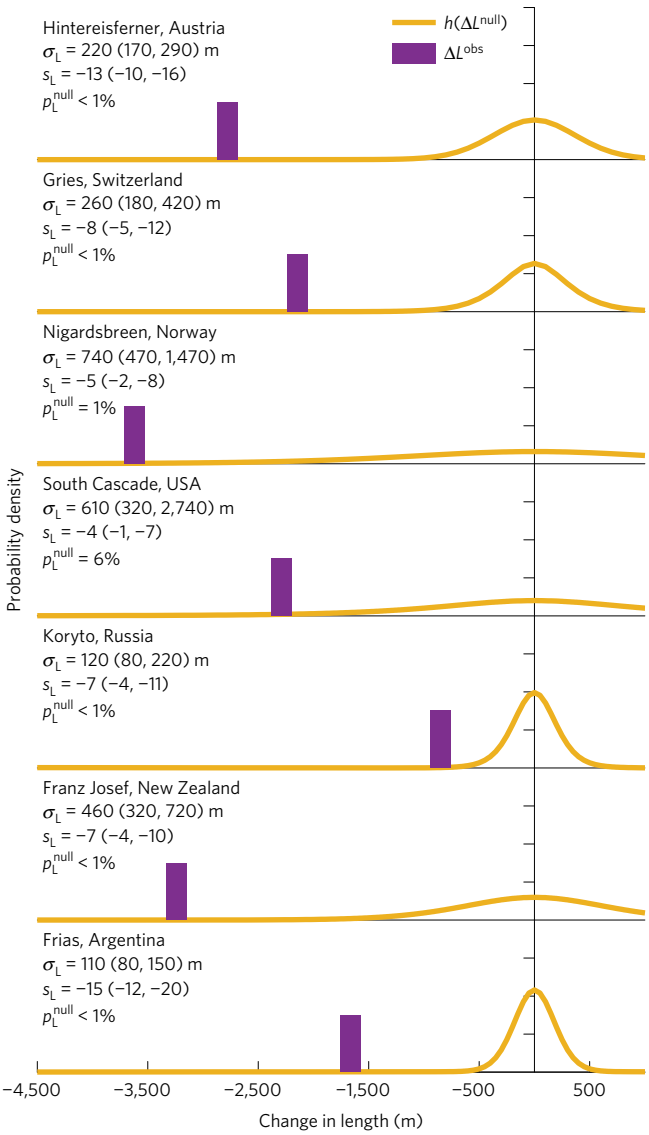

Figure 4 | Analysis of glacier retreat from around the world (see Fig. 1). For each glacier, the PDF for ΔL in any 130-yr period with no climate change is shown, and compared with the observed retreat represented by the vertical bar. Also given is the estimated standard deviation and signal-to-noise ratio (with 95% bounds), and the p value for the null hypothesis—the likelihood that the observed retreat occurred in the absence of a climate change. All PDFs have areas normalized to 1. See Supplementary Information for 30 other glaciers worldwide, and a full table of the analyses.

(Methods). Finally, we test against a null hypothesis of no climate change. Using equation (1), the probability distribution of a given ΔL occurring in any 130-yr period without climate change comes from combining the PDFs for each of the terms on the right-hand side of: $\Delta L|^{null} = \sigma_L \cdot \gamma \cdot s_b|^{null}$, where the PDF for $s_b|^{null}$ comes from the detrended mass-balance observations (Methods). We find the probability that the observed retreat comes from the null distribution is minuscule ($p_L^{null} = 0.001\%$, Fig. 4a); it is thus highly significant and must be attributed to a climate change. In general, the statistical significance of the glacier retreat may be larger or smaller than that of other local climate metrics. For example, although the global aggregate of the much shorter duration glacier mass-balance observations is negative and significant at the 5% level[7], only 17/48 and 4/48 of the individual summer and winter mass-balance records longer than 10 years exhibit significant trends (all negative)[7]. For Hintereisferner, s_L and the statistical significance are so large because of the observed drying in addition to the observed warming (Fig. 3a,b), and because the Bayesian step combining PDFs with length observations indicates a slightly more negative s_L (Fig. 3e).

An evaluation of glaciers worldwide

The foregoing analysis can be applied to any glacier with a long length record and known mass-balance variability. The results for seven widely distributed glaciers (Fig. 1) are shown in Fig. 4. Although the size of the retreats vary by more than a factor of five, for each glacier it is very unlikely that it could have occurred without climate forcing. The least significant retreat, $p_L^{null} = 6\%$, is South Cascade Glacier, which has a small median $s_b \simeq -0.7$, resulting from a relatively small warming in a maritime climate where winter mass-balance variability exceeds that in summer[7] (Supplementary Information).

We have analysed a total of 37 glaciers worldwide, selecting those with the longest mass-balance and length records. All steps and results are detailed in the Methods and Supplementary Information. In several cases, nearby mass-balance records were used, and when length observations were too sparse to characterize the degrees of freedom, a uniform negative-definite $h_{s_L}|^{L^{obs}}$ was assumed, consistent with the observed retreat (that is, $\Delta L < 0$) of all evaluated glaciers (Fig. 1 and Supplementary Information), and the fact that σ_L is positive. For the 37 glaciers, the median values of s_L and σ_L range from −2 to −15 and from 120 m to 750 m, respectively. Our analyses represent an approximately tenfold increase in the number of glaciers for which σ_L has been estimated; three of our selected glaciers have previous model-based estimates of σ_L that lie within our observation-based ranges[8,14]. Such estimates are valuable for putting reconstructions of past Holocene glacier fluctuations into context[15]. We note that the response of glacier length to climate trends and to natural variability form complementary pairs: glaciers that are sensitive to climate change also tend to have higher variability.

For 21 of the 37 glaciers, $p_L^{null} \leq 1\%$. Adopting IPCC nomenclature, it is thus 'virtually certain' that the retreat of each of these individual glaciers required a climate change. A further seven have $p_L^{null} \leq 5\%$. The least significant, Rabots Glacier in northern Sweden, has $p_L^{null} = 11\%$. Thus, for all but one glacier, it is 'very likely' (≥90%, IPCC) their retreat is attributable to climate change.

These calculations and uncertainty estimates can undoubtedly be refined and improved by more sophisticated mass-balance models and by detailed numerical case studies with explicit valley geometry, and of course our analyses do not, on their own, speak to the cause of the required climate change. However, the decadal response time of glaciers means their centennial retreat is predominantly a response to the twentieth-century climate trends rather than being a dynamical recovery from any antecedent conditions, such as the putative Little Ice Age[21]. The fundamental principle evinced here—that glaciers act as several-fold amplifiers of the signal-to-noise ratio of local climate trends—is robust. The principle is not limited to glaciers. Any component of the climate system with a decadal timescale will damp high-frequency variations and integrate centennial-scale trends. However, glaciers are perhaps unique in combining a decadal timescale with a strong sensitivity and simple dynamical response to temperature, creating near-maximum signal-to-noise ratios for centennial-scale climate change (Fig. 2b). In combination with climate and glacier observations, this has enabled our quantification of just how far individual glaciers have been driven from their pre-industrial states by climate change.

Methods

Methods, including statements of data availability and any associated accession codes and references, are available in the online version of this paper.

Received 21 September 2016; accepted 18 November 2016; published online 12 December 2016

References

1. Nussbaumer, S. U. & Zumbühl, H. J. The little ice age history of the glacier des Bosons (Mont Blonc massif, France): a new high-resolution glacier length curve based on historical documents. *Climatic Change* **111,** 301–334 (2012).
2. Forbes, J. D. *Occasional Papers on the Theory of Glaciers* (A & C Black, 1859).
3. Tyndall, J. & Huxley, T. H. Observations on Glaciers. *Proc. R. Soc. Lond.* **8,** 331–338 (1857).
4. Solomina, O. N. *et al*. Holocene glacier fluctuations. *Quat. Sci. Rev.* **111,** 9–34 (2015).
5. Leclercq, P. W. *et al*. A data set of world-wide glacier length fluctuations. *Cryosphere* **8,** 659–672 (2014).
6. Braithwaite, R. J. & Zhang, Y. Relationships between interannual variability of glacier mass balance and climate. *J. Glaciol.* **45,** 456–462 (1999).
7. Medwedeff, W. G. & Roe, G. H. Trends and variability in the global dataset of glacier mass balance. *Clim. Dynam.* http://dx.doi.org/10.1007/s00382-016-3253-x (2016).
8. Oerlemans, J. Holocene glacier fluctuations: is the current rate of retreat exceptional? *Ann. Glaciol.* **31,** 39–44 (2000).
9. Marzeion, B., Cogley, J. G., Richter, K. & Parkes, D. Attribution of global glacier mass loss to anthropogenic and natural causes. *Science* **345,** 919–921 (2014).
10. Leclercq, P. W. & Oerlemans, J. Global and hemispheric temperature reconstruction from glacier length fluctuations. *Clim. Dynam.* **38,** 1065–1079 (2012).
11. Bindoff, N. L. *et al*. in *Climate Change 2013: The Physical Science Basis* (eds Stocker, T. F. *et al*.) Ch. 10 (IPCC, Cambridge Univ. Press, 2013).
12. Jóhannesson, T., Raymond, C. F. & Waddington, E. D. Timescale for adjustments of glaciers to changes in mass balance. *J. Glaciol.* **35,** 355–369 (1989).
13. Oerlemans, J. *Glaciers and Climate Change* (A. A. Balkema, 2000).
14. Roe, G. H. & Baker, M. B. Glacier response to climate perturbations: an accurate linear geometric model. *J. Glaciol.* **60,** 670–684 (2014).
15. Anderson, L. S., Roe, G. H. & Anderson, R. S. The effects of interannual climate variability on paleoclimate estimates derived from glacial moraines. *Geology* **42,** 55–58 (2014).
16. Rohde, R. *et al*. A new estimate of the average earth surface land temperature spanning 1753 to 2011. *Geoinfor. Geostat.* http://dx.doi.org/10.4172/gigs.1000101 (2013).
17. Legates, D. R. & Willmott, C. J. Mean seasonal and spatial variability in gauge corrected global precipitation. *Int. J. Climatol.* **10,** 111–127 (1990).
18. *Fluctuations of Glaciers Database* (World Glacier Monitoring Service (2014); http://dx.doi.org/10.5904/wgms-fog-2014-09
19. Greuell, W. Hintereisferner, Austria: mass-balance reconstruction and numerical modelling of the historical length variations. *J. Glaciol.* **38,** 233–244 (1992).
20. Annan, J. D. & Hargreaves, J. C. Using multiple observationally-based constraints to estimate climate sensitivity. *Geophys. Res. Lett.* **33,** L06704 (2006).
21. Matthews, J. A. & Briffa, K. R. The little ice age: re-evaluation of an evolving concept. *Geogr. Ann.* **87 A,** 17–36 (2005).

Acknowledgements

We are grateful to P. Green, K. Armour, D. Battisti and E. Steig for valuable comments and conversations. F.H. thanks the Institute of Atmospheric and Cryospheric Sciences, University of Innsbruck for financial support.

Author contributions

G.H.R., M.B.B. and F.H. planned the analyses, which G.H.R. performed. All authors contributed to the interpretation of the results and to writing the manuscript.

Additional information

Supplementary information is available in the online version of the paper. Reprints and permissions information is available online at www.nature.com/reprints. Correspondence and requests for materials should be addressed to G.H.R.

Competing financial interests

The authors declare no competing financial interests.

Methods

A three-stage model. A refinement of earlier analytical glacier models[12,13] was developed in ref. 14, and showed that numerical models of ice flow on a constant slope could be accurately emulated by a third-order linear differential equation:

$$\left(\frac{\mathrm{d}}{\mathrm{d}t}+\frac{1}{\epsilon\tau}\right)^3 L' = \frac{\beta}{\epsilon^3\tau^2}b'(t) \tag{3}$$

where $L'(t)$ is the length perturbation from some long-term, mean-state position, driven by mass-balance fluctuations, $b'(t)$. $\tau=-H/b_\mathrm{t}$, where H is a characteristic thickness and b_t is the (negative) mass balance at the terminus; $\beta=A_\mathrm{tot}/(wH)$, where A_tot is the mean-state glacier area and w is the characteristic width at the terminus; and $\epsilon=1/\sqrt{3}$. Reference 14 showed that equation (3) captures three essential stages of glacier adjustment: changes in interior ice thickness drive changes in ice flux at the terminus that, in turn, drive changes in glacier length. Equation (3) has analytic solutions that facilitate efficient analyses over a wide range of parameter space.

Response to a trend. Consider a linear trend in mass balance commencing at $t=0$. Let $\Delta b(t_\mathrm{o})$ be the resulting change in mass balance after a time t_o has elapsed. The exact solution of equation (3) for the resulting length change, $\Delta L(t_\mathrm{o})$, is:

$$\Delta L(t_\mathrm{o}) = \phi(t_\mathrm{o},\tau)\cdot\beta\cdot\Delta b(t_\mathrm{o}) \tag{4}$$

where

$$\phi(t_\mathrm{o},\tau)=\tau\left[\frac{3}{r}(\mathrm{e}^{-r}-1)+1+\mathrm{e}^{-r}\left(\frac{r}{2}+2\right)\right] \tag{5}$$

and $r=t_\mathrm{o}/\epsilon\tau$. We note that $\phi(t_\mathrm{o},\tau)\to\frac{\tau}{t_\mathrm{o}}(t_\mathrm{o}-3\epsilon\tau)$ in the limit that $t_0\gg\epsilon\tau$. Equation (4) is used to calculate the curves in Fig. 2a.

Glacier-length variance. Consider stochastic white-noise interannual fluctuations in mass balance (that is, random, year-to-year variability due to the vagaries of the weather, with no year-to-year persistence). Let the standard deviation of such fluctuations be σ_b. Such mass-balance fluctuations drive variability in glacier length, characterized by a standard deviation σ_L. Ref. 14 shows that:

$$\sigma_\mathrm{L}=\beta\cdot\psi(\tau)\cdot\sigma_\mathrm{b} \tag{6}$$

where

$$\psi(\tau)=\tau\left\{\frac{(1-\kappa)(1+4\kappa^2+\kappa^4)}{(1+\kappa)^5}\right\}^{\frac{1}{2}} \tag{7}$$

with $\kappa=1-(\Delta t/\epsilon\tau)$ and $\Delta t=1$ yr. We note that $\psi(\tau)\to(3\tau\Delta t/16\epsilon)^{1/2}$ in the limit of $\epsilon\tau\gg\Delta t$.

Estimated variance for Hintereisferner. Taking Hintereisferner in the Austrian Alps as an example, reasonable values for parameters are[19]: $A_\mathrm{tot}\simeq10.5\,\mathrm{km}^2$, $w\simeq400$ m, $H\simeq170$ m; $b_\mathrm{t}\simeq-6.5\,\mathrm{m\,yr}^{-1}$, giving $\beta\simeq150$ and $\tau\simeq30$ yr. With $\sigma_\mathrm{b}\simeq0.5\,\mathrm{m\,yr}^{-1}$ from the adjacent Vernagtferner[7,18], equation (6) yields $\sigma_\mathrm{L}\simeq230$ m. This value is close to the central estimate of σ_L made from observed retreat of Hintereisferner and local climate trends: $\sigma_\mathrm{L}\simeq220$ m (Fig. 4).

Signal-to-noise ratio, s_L. Therefore, for a climate trend superposed on natural interannual variability, the signal-to-noise ratio for glacier length, s_L, can be formed from equation (4) divided by equation (6):

$$s_\mathrm{L}=\frac{\Delta L}{\sigma_\mathrm{L}}=\frac{\phi(t_\mathrm{o},\tau)}{\psi(\tau)}\cdot\frac{\Delta b(t_\mathrm{o})}{\sigma_\mathrm{b}}=\gamma(t_\mathrm{o},\tau)\cdot s_\mathrm{b} \tag{8}$$

Contours of $\gamma(t_\mathrm{o},\tau)$ are plotted in Fig. 2b.

Signal-to-noise ratio from length observations. We considered glacier records from a compilation of 471 glacier-length histories worldwide[5]. The data set uses Stineman interpolation in between individual length observations to produce annual time series, although our results are not sensitive to the interpolation method. We selected 37 glaciers in total (in each of five regions—see Supplementary Information), and focus on the period 1880 to 2010. The main criteria in selecting glaciers were long mass-balance records and a broad geographic distribution. However, we also preferentially selected glaciers with near-continuous length observations, although for some regions such as Asia and South America, this criterion could not always be met.

The signal-to-noise ratio is given by $s_\mathrm{L}=\Delta L/\sigma_\mathrm{L}$, where ΔL is the change in length and σ_L is the standard deviation of the variability about that trend. We estimate s_L from least-squares linear regression. Let $h_{s_\mathrm{L}}(s_\mathrm{L})|^{L_\mathrm{obs}}$ be the probability density function (PDF) of s_L, and let $\overline{\Delta L}$ and $\overline{\sigma_\mathrm{L}}$ be the central estimates of ΔL and σ_L, respectively. From ref. 22, and the standard formulae for uncertainties in regression parameters[23] applied to glacier trends[24], it can be shown that:

$$h_{s_\mathrm{L}}(s_\mathrm{L})|^{L_\mathrm{obs}}=\sqrt{\frac{\nu-1}{12}}\,\mathcal{F}\left(\sqrt{\frac{\nu-1}{12}}s_\mathrm{L},\nu-1,\frac{\overline{\Delta L}}{\overline{\sigma_\mathrm{L}}}\sqrt{\frac{\nu-1}{12}}\right) \tag{9}$$

where $\mathcal{F}(x,\nu-1,\mu)$ is a non-central t-distribution of the variable x with $\nu-1$ degrees of freedom, and non-centrality parameter μ (refs 22,24). The formula in equation (9) was verified in Monte Carlo simulations of time series with stipulated trends added to random realizations of noise.

Degrees of freedom in a record. We estimate the number of degrees of freedom, ν, in the glacier record following a procedure recommended in ref. 23. We fit a third-order autoregressive process to the length data[14,23,25] and calculate the associated autocorrelation function, $r(\tau)$. The effective degrees of freedom are then given by:

$$\nu=\frac{n\Delta t}{\Delta t+2\int_0^\infty r(\tau)\mathrm{d}\tau} \tag{10}$$

where n is the number of years in the record and $\Delta t=1$ yr. The number of degrees of freedom in the length observations ranges from <1 up to ~6. Low degrees of freedom yield broad distributions for $h_{s_\mathrm{L}}|^{L_\mathrm{obs}}$ (for example, Fig. 3e), so that the most important information from the length observations is only that s_L is not positive. When this method identifies $\nu\leq1$, or when the length records are sparse, $h_{s_\mathrm{L}}|^{L_\mathrm{obs}}$ cannot be calculated in this way. We instead stipulate a uniform negative-definite $h_{s_\mathrm{L}}|^{L_\mathrm{obs}}$, consistent with the observed retreat (that is, $\Delta L<0$) of all glaciers analysed and the fact that σ_L is positive definite (see also Supplementary Information). Our second method for calculating s_L (described below) uses climate observations with many more degrees of freedom, which produces a much narrower PDF (for example, Fig. 3e). When the two PDFs are combined, the narrower PDF dominates (Fig. 3e), and so our results and conclusions are not sensitive to the estimate of ν.

Signal-to-noise ratio from climate observations and glacier amplification factor. The second method for calculating s_L is to use the relationship from equation (8):

$$s_\mathrm{L}=\gamma(t_\mathrm{o},\tau)\cdot s_\mathrm{b} \tag{11}$$

Calculating s_b and its persistence. As described in the main text, the mass-balance model is:

$$b'(t)=b'_\mathrm{w}(t)+b'_\mathrm{s}(t)=\sigma_{b_\mathrm{w}}\frac{P'(t)}{\sigma_\mathrm{P}}+\sigma_{b_\mathrm{s}}\frac{T'(t)}{\sigma_\mathrm{T}} \tag{12}$$

Values of P' (annual mean) come from the Legates and Willmot data set[17]. Values of T' (June to September in the Northern Hemisphere extratropics, December to March in Southern Hemisphere extratropics; annual mean in the tropics) come from the Berkeley Earth data set[16]. The data were taken from the nearest land grid point to each glacier's location. The data sets were chosen for their high spatial resolution, but alternative data sets show similar trends.

The PDF of s_b ($\equiv h_{s_\mathrm{b}}$) is calculated using the same non-central t-distribution as equation (9):

$$h_{s_\mathrm{b}}(s_\mathrm{b})|^{T,P_\mathrm{obs}}=\sqrt{\frac{\nu-1}{12}}\,\mathcal{F}\left(\sqrt{\frac{\nu-1}{12}}s_\mathrm{L},\nu-1,\frac{\overline{\Delta b}}{\overline{\sigma_\mathrm{b}}}\sqrt{\frac{\nu-1}{12}}\right) \tag{13}$$

Here, the degrees of freedom are also calculated by fitting an autoregressive model to $b'(t)$. Only 3 out of the 37 glaciers analysed have a mass-balance time series that indicates any persistence (documented in the Supplementary Spreadsheet), with most being well characterized by white noise, consistent with mass-balance observations[7,26]. Thus, for almost all of the records, the degrees of freedom are equal to the number of years in the record. The majority of the mass-balance trends are dominated by trends in summer mass balance due to the melt-season temperature trends, which is also seen in the much shorter records of actual glacier mass balance[7].

Calculating the PDF of γ from the PDF of τ. The central estimate of τ comes from the relationship $\tau=-H/b_\mathrm{t}$. For each glacier, the source references for the characteristic thickness H and terminus ablation rate b_t are given in the Supplementary Spreadsheet. For the PDF of uncertainty in τ ($\equiv h_\tau(\tau)$) we take a gamma distribution (ensuring τ is positive definite), with a standard deviation of $\tau/4$ (Fig. 3d). Thus, the 95% uncertainty bounds on τ (that is, $\pm2\sigma$) are equal to τ itself—a broad and thus conservative estimate of the uncertainty.

The PDF of $\gamma(t_o,\tau)$ ($\equiv h_\gamma$) comes from equation (8), and applying the relationship:

$$h_\gamma(\gamma)=\frac{h_\tau(\tau)}{\partial\gamma/\partial\tau} \tag{14}$$

For our analyses $t_o=130$ yr (1880 to 2010). The nature of γ is such that even very broad PDFs in τ map onto narrow PDFs of γ (Fig. 3d).

The PDF of s_L. Finally, the PDF of s_L ($\equiv h_{s_L}(s_L)|^{T,P_{obs}}$) comes from combining h_γ and h_{s_b}. The probability that s_L lies between any given value s_L and s_L+ds_L is given by:

$$h_{s_L}(s_L)\mathrm{d}s_L=\sum h_\gamma(\gamma)\mathrm{d}\gamma\cdot h_{s_b}(s_b)\mathrm{d}s_b \tag{15}$$

where the sum is taken over all possible pairs (s_b,γ) for which $s_b\cdot\gamma=s_L$. Using $\mathrm{d}s_b/\mathrm{d}s_L=1/\gamma$, and taking the limits that $\mathrm{d}s_L,\mathrm{d}\gamma,\mathrm{d}s_b\to 0$, the sum becomes an integral:

$$h_{s_L}(s_L)|^{T,P_{obs}}=\int_0^\infty h_\gamma(\gamma)\cdot h_{s_b}(s_L/\gamma)\cdot\frac{1}{\gamma}\cdot\mathrm{d}\gamma \tag{16}$$

In other analyses in this study, the PDFs for all variables that are the product or ratio of two other variables are generated in a similar fashion. Where noted, the PDFs generated in this way have been verified with Monte Carlo simulations.

Combining the PDFs for s_L using Bayes' theorem. $h_{s_L}|^{L_{obs}}$ and $h_{s_L}|^{T,P_{obs}}$ are independent and so can be combined using Bayes' theorem to yield an updated, posterior PDF for s_L. We regard $h_{s_L}|^{L_{obs}}$ as the prior PDF that is updated by new information from the observed s_b. $h_{s_L}|^{T,P_{obs}}$ is equivalent to the likelihood function $\mathcal{L}(s_L|s_b)$, the likelihood of s_L given the new information s_b (ref. 20). For glaciers whose length history is too sparse (meaning if there are temporal gaps in the observations that are comparable to τ) or if the degrees of freedom are less than one, we stipulate an uninformative, flat prior for $h_{s_L}|^{L_{obs}}$ that is negative definite: $h_{s_L}=$ constant for $s_L<0$, and $h_{s_L}=0$ otherwise. This is consistent with the observed negative ΔL of all glaciers analysed and the fact that σ_L is positive definite (see also Supplementary Information). Then the posterior PDF for s_L is given by:

$$h_{s_L}(s_L)|^{post}=k\cdot h_{s_L}(s_L)|^{L_{obs}}\cdot h_{s_L}(s_L)|^{T,P_{obs}} \tag{17}$$

where k is a normalization constant independent of s_L. An example of $h_{s_L}(s_L)|^{post}$ for Hintereisferner is shown in Fig. 3e.

Estimating σ_L from s_L. We estimate the PDF of σ_L ($\equiv h_{\sigma_L}$) from the relationship:

$$\sigma_L=\frac{\overline{\Delta L}}{s_L} \tag{18}$$

using $h_{s_L}|^{post}$ (that is, equation (17)) and the fact that ΔL is well constrained from observations.

Generating the PDF of the null hypothesis $p_L|^{null}$. We evaluate the observed glacier retreat against a null hypothesis of no climate change. For no climate trend the PDF of s_b ($\equiv h_{s_b}|^{null}$) is governed by the standard Student's t-distribution centred on zero[24]. That is, equation (13) with $\overline{\Delta b}=0$. Thus, the PDF of the null hypothesis for s_L, $h_{s_L}|^{null}$, is calculated from the relationship $s_L=\gamma\cdot s_b$ and combining h_γ and $h_{s_L}|^{null}$.

Finally, we have $\Delta L=\sigma_L\cdot s_L$, and so the PDF of the null hypothesis for ΔL ($\equiv h_{\Delta L}|^{null}$) comes from combining h_{σ_L} and $h_{s_L}|^{null}$. We confirmed the validity of our calculations of $h_{\Delta L}|^{null}$ by Monte Carlo methods: generating a PDF of ΔLs from 10,000 130-yr integrations of the three-stage glacier-length model driven by climate variability with no trend.

Examples for $h_{\Delta L}|^{null}$ are shown in Fig. 4 and in Supplementary Figs 3–8. Following the standard approach, we determine the statistical significance of a glacier's retreat by calculating the probability, $p_L|^{null}$, that a ΔL could be consistent with the null hypothesis and yet lie beyond the observed retreat.

Code availability. The three-stage glacier model code is available from: http://earthweb.ess.washington.edu/roe/GerardWeb/Home.html. All analyses were performed by implementing the equations presented in the paper, for the data sets documented above.

Data availability. The following data sets were used in this study: glacier mass balance from: http://dx.doi.org/10.5904/wgms-fog-2014-09; glacier mass-balance analysis from: doi:10.1007/s00382-016-3253-x; glacier-length records from: http://www.the-cryosphere.net/8/659/2014/tc-8-659-2014-supplement.zip; Legates and Willmott precipitation data available from: http://www.esrl.noaa.gov/psd/data/gridded/data.UDel_AirT_Precip.html; Berkeley Earth temperature data available from: http://www.berkeleyearth.org/data. Other glacier parameters were taken from studies cited in the paper, and are documented in the Supplementary Information and in an accompanying spreadsheet.

References

22. Nadarajah, S. & Kotz, S. Computation of signal-to-noise ratios. *Commun. Math. Comput. Chem.* **57,** 105–110 (2007).
23. von Storch, H. & Zwiers, F. W. *Statistical Analysis in Climate Research* (Cambridge Univ. Press, 1999).
24. Roe, G. H. What do glaciers tell us about climate variability and climate change? *J. Glaciol.* **57,** 567–578 (2011).
25. Schneider, T. & Neumaier, A. Algorithm 808: ARFIT—a Matlab package for the estimation of parameters and eigenmodes of multivariate autoregressive models. *ACM Trans. Math. Softw.* **27,** 58–65 (2001).
26. Burke, E. E. & Roe, G. H. The persistence of memory in the climatic forcing of glaciers. *Clim. Dynam.* **42,** 1335–1346 (2014).